Al-Rafidain Journal of Engineering Sciences

Journal homepage https://rjes.iq/index.php/rjes

ISSN 3005-3153 (Online)

Nonlinear Finite Element Modeling and Experimental Evaluation of Reinforced Foamed Concrete T-Beams

Wahage I. Abdul-Kareem[1,*] , Nagham Tariq Al-shafi'i[2] , Zainab Mohammed Ali[3]

[1,2]Department of Civil Engineering, College of Engineering, Al-Mustansiriyah University, Baghdad, Iraq.

[3]Highway and Transportation Engineering Department, College of Engineering, Al-Mustansiriyah University, Baghdad, Iraq.

ARTICLE INFO

Article history:
Received 05-06-2026
Revised 05-06-2026,
Accepted 20-06-2026,
Available online 22-06-2026

Keywords:
Foamed Concrete
T-beams
Finite Element
ABAQUS
Numerical Results

ABSTRACT

This study focuses on the structural behavior of reinforced foamed concrete T-beams, based on both experimental and theoretical/numerical comparisons by using ABAQUS software. The Concrete Damage Plasticity (CDP) model was employed to model the nonlinear behavior of foamed concrete T-beams, and the steel reinforcement was represented as an embedded truss element. The experimental results were used to validate the numerical results for ultimate load capacity, mid-span deflection, load-deflection response, and crack pattern. A good agreement between the experimental and numerical results was obtained. The average experimental ultimate load was 129.08 kN, and the average numerical ultimate load was 131.78 kN. A parametric study was conducted to simulate the response of foamed concrete T-beams subjected to a uniformly distributed load. Findings showed that distributed loading successfully increased load-carrying capacity and minimized deflection, thereby improving structural performance. Thus, the developed numerical model can be considered well validated for predicting the behavior of fiber-reinforced concrete T-beams and for conducting parametric studies.

1. Introduction

In recent years, lightweight concrete has been widely used in construction due to its innovative and economic advantages, most often in structural components. Lightweight concrete has a lower density than conventional concrete, which helps reduce the total dead load on the structure. This reduction in structural weight can lead to smaller column and foundation dimensions and help avoid heavy load-bearing components [1]. Foamed concrete (FC) is a lightweight form of concrete that can be produced with or without using fine aggregates. It consists of a high void space ratio and cement binders. Foamed concrete density ranges from 400 to 1850 kg/m³. Structural lightweight concrete has a density of 1350–1900 kg/m^3, whereas non-structural lightweight concrete may be as low as 300–800 kg/m^3.[5] Structural lightweight foamed concrete has proven beneficial compared to regular weight concrete due to its high strength and durability [2].

The use of supplementary cementitious materials (SCMs), such as silica fume, has been shown to enhance the characteristics of foam

Corresponding author E-mail address: wahageibrahim@uomustansiriyah.edu.iq
https://doi.org/10.61268/03fv6m15

concrete through pozzolanic reactions and micro-filling effects, which densify the cementitious matrix and refine the pore structure, thereby improving the long-term durability of FC [3]. Additionally, the inclusion of randomly oriented fibers in foamed concrete enhances load transfer, compressive strength, tensile strength, and ductility by transforming typical brittle behavior to elastic-plastic behavior [4].

When floor slabs and their supporting beams are poured together as a single unit, they exhibit deflection under external loads, similar to that of the beams. T-section beams, known for their straightforward construction and cost-effectiveness, have been widely employed in flooring systems. They are a practical and efficient construction method [5,6]. Confirming an effective connection between the slab and the drop beam is important for classifying a T-section beam. The connection must consistently withstand longitudinal and transverse flexural stresses [7].

Marcin et al. (2016) published the results of a numerical study on the fracture behavior of initially notched beams produced from foamed concrete by using the Extended Finite Element Method (XFEM). Numerical models correctly simulated the fracture behavior of beams noticed during testing. By comparison experiments and computer simulations, XFEM techniques provided acceptable approximations of the load-bearing capacity and damage processes of beams constructed from FC, which offered a certain basis for realistic structural applications [8]. Historically, the Romans were pioneers in using animal blood mixed with gravel, sand, water, and heated lime, which produced tiny air bubbles that enhanced the mixture's durability [9]

(Harry and Udoh, 2016) presented a numerical study on the effect of flange width on the flexural behavior of a reinforced concrete T-section beam. Three different flange widths, which include 200, 400, and 600mm, were considered in this study. The result showed that the stiffness of the beam increased with increasing flange width. The flange width influenced the initial cracking load. The wider the flange width, the higher the cracking load. The results, in terms of mid-span deflection and crack pattern, showed no appreciable difference among the different flange widths considered in this study. Additionally, the findings illustrated that the finite element model can properly model a reinforced concrete T-beam. Additionally, the load, deflection, and strain values from the experimental test compared favorably with those from finite element model [10].

2. Research Gap

The fundamental motivation of this work is the lack of studies that validate theoretical predictions against actual experimental behavior of fiber foam reinforced concrete T-beams. Most analytical models are developed for normal-weight concrete and may not reflect differences in the mechanical behavior of foam concrete, particularly its high porosity and lower density. Therefore, these theoretical methods for predicting key structural responses, such as load capacity, deflection, and failure mode, remain unverified in terms of reliability and accuracy.

3. Objective

To develop and validate an ABAQUS model against experimental results before using this validated model in a parametric study.

4. Novel Contribution

A numerically calibrated method to predict the behavior of fibered foam reinforced

concrete as a T-beam under two-concentrated and uniformly distributed loading.

5. Expected Outcomes

The model should predict strength, serviceability, cracking, and failure response, and illustrate the effects of the longitudinal reinforcement ratio, the flange-to-web width ratio, and the load distribution.

6. Methodology

The objective of this paper is to compare the experimental results obtained in tests on reinforced foamed concrete T-beams with theoretical/numerical results. This comparison evaluated the capability of the theoretical model to predict ultimate load, midspan deflection, load-deflection response, crack pattern, and failure mode of tested beams. Table 1 illustrates the mix proportions of foamed concrete T-beams.

Table 1: Mix Proportion of Foamed Concrete T-beams

Cement (kg/m^3)	Sand (kg/m^3)	Silica Fume* (%)	Water (kg/m^3)	Superplasticizer**	w/c	Foam (kg/m^3)	Steel Fibers***
745	745	10	262.50	1.60	0.32	20	0.50

*(%) by weight of cement
** (%) by weight of total cementitious materials
*** (%) by mix volume

The tested beams were divided into subgroups based on the main variables studied. In Group 1, beams B-1, B-2, and B-3 had longitudinal reinforcement ratios of ρw = 0.00864, 0.00597, and 0.01551, respectively. In this group, the shear span-to-effective depth ratio, a/d, is constant at 2.6, and the flange-to-web width ratio, bf/bw, is fixed at 2.083. Consequently, this group was used to investigate the influence of reinforcement ratio on the characteristics of foamed concrete T-beams.

Group 2 consisted of beams B-1, B-4, B-5, and B-6 for which the flange-to-web width ratio bf/bw was set to 2.083, 2.5, 2.916, and 0, respectively. This group had a constant reinforcement ratio of 0.00864, and the a/d ratio was set to 2.6. This sample was taken to study the influence of flange width on the load-carrying performance of beams.

The theoretical/numerical model was developed using the same geometry, reinforcement details, material properties, loading arrangement, and support conditions adopted in the experimental work. The experimental findings were then used as benchmark data to align the theoretical predictions. Agreement was assessed based on ultimate load, deflection, load–deflection behavior, and crack pattern.

Table 2: The Details of Tested Beams

Beams	ρw	a/d	bf/bw
Group no.1			
B-1	0.00864	2.6	2.083
B-2	0.00597	2.6	2.083
B-3	0.01551	2.6	2.083
Group no.2			
B-1	0.00864	2.6	2.083
B-4	0.00864	2.6	2.500
B-5	0.00864	2.6	2.916
B-6	0.00864	2.6	0

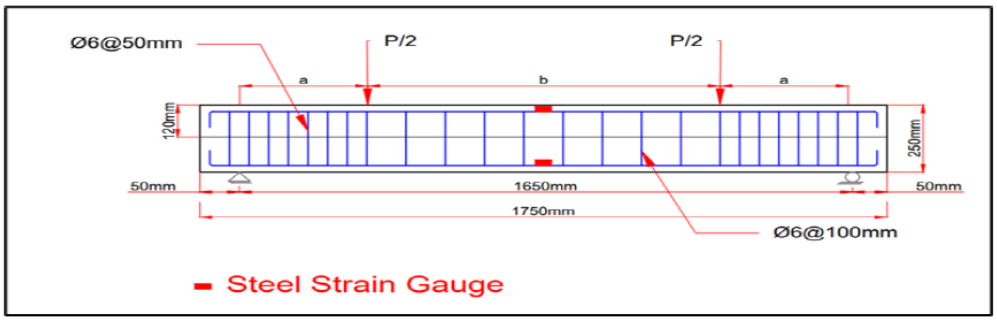

Figure 1. Reinforcement Details of FC T-beam

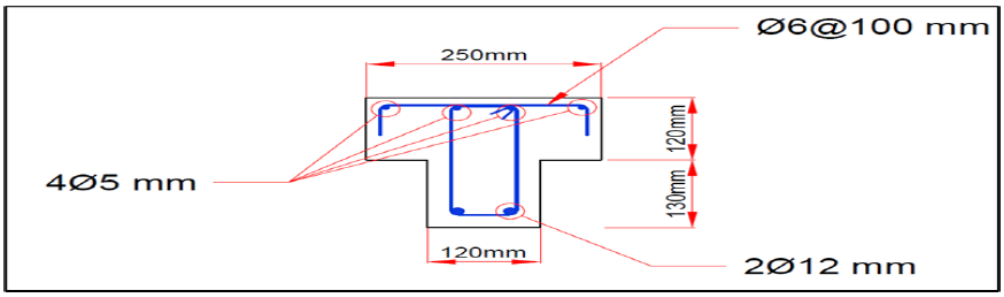

Figure 2. Typical Section of Reference FC T-beam

6.1 Numerical Model Procedure

The finite element model of the reinforced concrete T-beams was developed using ABAQUS to simulate their structural response under applied loading. The modeling procedure involved defining the beam geometry, specifying material properties, and employing the Concrete Damage Plasticity (CDP) model to capture concrete's nonlinear response. The CDP parameters were established from both experimentally obtained material properties and literature values. The elastic and non-linear stress–strain responses in tension and compression were taken from the Seanz constitutive model, while the remaining parameters, such as dilation angle, eccentricity, and viscosity, were calibrated to ensure numerical stability and to replicate the experimental load–deflection behavior of foamed concrete T-beams. After all model components were assembled, the loading conditions, boundary constraints, and interaction properties were defined. An appropriate mesh was then generated to ensure numerical convergence and accuracy of the analysis. Finally, the obtained simulation results, including deformation, stress distribution, and failure behavior, were evaluated.

6.2 Concrete Modeling

The concrete was modeled as the primary structural element using an 8-node linear brick element (C3D8I) in ABAQUS software to represent a deformable solid. For the constitutive behavior, the nonlinear response of concrete was simulated using the Concrete Damage Plasticity (CDP) model. The material modeling parameters were defined based on the experimental results, yielding a mean modulus of elasticity of 20.5 GPa. Concrete compressive and tensile behaviors were defined using the relationships

Corresponding author E-mail address: wahageibrahim@uomustansiriyah.edu.iq
https://doi.org/10.61268/03fv6m15

proposed by Seanz [11] and Hsu [12], respectively, calibrated against experimental data. Appropriate selection of CDP parameters, especially the dilation angle and viscosity, was used to enhance convergence and avoid numerical instability. A viscosity parameter of 0.0003 was used in the analysis; see Table 3.

Table 3: Concrete Damage Plasticity: Parameters Used for Calibrating the Model

Young's modulus	20.5 GPa
Poison's ratio	0.19
Dilation angle	40°
Eccentricity	0.1
fbo=fco	1.16
K	0.667
Viscosity parameter	0.0003
Compressive behavior	Proposed by Seanz [11] and Hsu [12]
Compressive damage	
Tension behavior	
Tension damage	

6.3 Steel Reinforcement Modeling

In the numerical model, steel reinforcement was modeled using a 2-node wire-type truss element (T3D2) in ABAQUS. Data for the reinforcement configuration (bar diameter, length, and cross-sectional properties) were defined based on the geometry of the investigated T-beams, as defined in the property module.

The constitutive behavior of steel was defined based on the experimental results summarized in Table 4. The elastic response was characterized by a Young's modulus of 200 GPa and a Poisson's ratio of 0.3 for both stirrups and longitudinal bars.

For each bar diameter, the inelastic response was implemented using experimentally obtained yield and ultimate strengths, along with corresponding plastic strain values.

In this study, the steel was assumed to follow an elastic-perfectly plastic model, undergoing linear elasticity up to yielding, followed by a plastic plateau with no strain hardening. This assumption was made to simplify the numerical model and accurately represent the steel-concrete interaction behavior.

6.4 Modeling of Steel Plates and Supports

The loading and support plates were introduced in each numerical model to ensure the uniform distribution of applied loads over the specimen's contact surfaces and to prevent local stress concentrations in these regions. The modeling was performed

Table 4: Steel Reinforcement Characteristics

Model	**Longitudinal bar (16 mm)**	**Longitudinal bar (12 mm)**	**Longitudinal bar (10 mm)**	**Longitudinal bar (6 mm)**	**Longitudinal bar (5 mm)**
Density	7850 kg/m^3	7850 kg/m^3	7850 kg/m^3	7850 kg/m^3	7850 kg/m^3
Young modulus	200 GPa	200 GPa	200 GPa	200 GPa	200 GPa
Poisson ratio	0.3	0.3	0.3	0.3	0.3
fy	573 MPa	654 MPa	723 MPa	608 MPa	720 MPa
fu	667.33 MPa	741 MPa	803 MPa	608 MPa	720 MPa
Plastic strain at fy	0	0	0	0	0
Plastic strain at fu	0.177	0.152	0.102	0.150	0.165

in ABAQUS software using 8-node linear brick elements with reduced integration and hourglass control (C3D8R), which were defined as extrusion-type deformable solid parts. The dimensions adopted for the loading and support plates were 150 mm × 50 mm × 50 mm.

The steel plates were treated solely as load-transfer and boundary-conditioning elements; their mechanical response was assumed to be linearly elastic. This simplification reduced computational effort while maintaining adequate numerical accuracy.

Due to their high stiffness and negligible deformation under loading, modeling the plates as elastic bodies is sufficient and consistent with experimental conditions, in which the plates serve to distribute stresses uniformly and mitigate premature local failure at the contact interfaces.

6.5 Assembly

The assembly stage was performed to integrate the components of the numerical model in ABAQUS software into a single system, ensuring proper interaction among them. All parts were first placed in the global coordinate system and oriented to match the geometry of realistic specimens under a defined test configuration. The model components were positioned accurately relative to the concrete body and the predefined datum lines.

The steel reinforcement, consisting of longitudinal bars and stirrups, was assigned to their respective locations in the concrete model, following the reinforcement layout and spacing used for the experimental beams.

Support conditions were subsequently applied at the T-beam ends to simulate the experimental boundary conditions and to ensure the structure's stabilization during loading. Moreover, the loading plate was placed on the top face of the T-beam to simulate the actual load location, and measurement points were assigned as needed.

The assembly process provided a numerical model consistent with the physical test setup and accurately represented the structural response under loading.

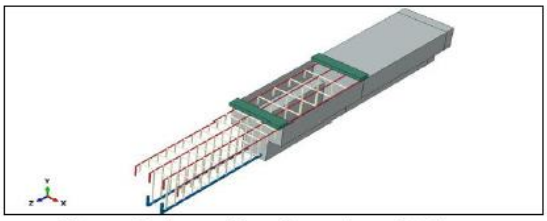

Figure 3. Assembly of specimen (B-1)

6.6 Stages of Loading

The analysis procedure in ABAQUS software was defined using a series of analysis steps to replicate the beams' gradual structural response under loading. An initial step was taken to define the model's boundary conditions and other settings using predefined values before applying any external load. Subsequently, a static general procedure employing an implicit solution scheme was applied to the loading-stage analysis, which is appropriate for nonlinear reinforced concrete with cracking and stiffness degradation.

The analysis employed automatic load incrementation to obtain stable, reliable results, which were then used to identify critical stress-concentration zones associated with potential failure zones. The increment size was based on the model's nonlinear response, thereby improving convergence and accurately capturing crack initiation and propagation throughout all loading stages. Multiple trial analyses were conducted to identify appropriate control settings, and a

total step time of 2 seconds was ultimately chosen to balance numerical accuracy and computational efficiency. An output interval of 0.02 seconds was used to record the structural response at smaller increments, enabling a more detailed assessment.

The adopted analysis procedure provided comprehensive information on the behavior and failure mechanisms of the tested T-beams, including results on stress distribution, displacement response, and reaction forces.

6.7 Finite Element Model Setup and Analysis Conditions

Defining appropriate contact interactions, constraints, loading, and boundary conditions is essential to ensure that the finite element model realistically represents the behavior of reinforced concrete beams under static loading. These definitions govern contact interaction between components, control force transfer, and improve the accuracy of predicted load transfer and stress distribution.

In this study, a surface-to-surface interaction was defined to model the contact behavior between interfaces using a penalty-based friction formulation. The coefficient of friction was set to 0.6, based on previous research, to represent the frictional resistance at the beam-support and loading contact surfaces, as these contact regions play a significant role in load transfer and overall structural performance.

For normal behavior, hard contact was assigned to prevent penetration between contacting surfaces while allowing separation when required, a widely used approach in finite element modeling of reinforced concrete members to simulate a contact without assuming perfect bonding. After defining these parameters, the interaction was assigned to the relevant surfaces, as shown in Figure 4, thereby improving the representation of stress distribution and cracking behavior.

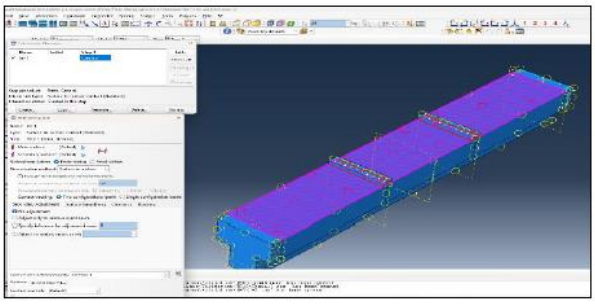

Figure 4. Interaction (surface to surface)

To represent the composite action between reinforcement and concrete, an embedded region with a perfect bond between steel and concrete was used to ensure full compatibility between the steel bars and the surrounding concrete, so that both deform together without relative slip, as shown in Figure 5.

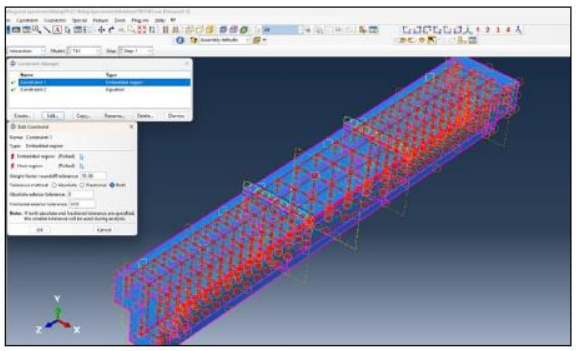

Figure 5. Constraint (Embedded Region)

In addition, an equation constraint was introduced in the loading region, as shown in Figure 6, to ensure uniform displacement across the loading plate by mathematically coupling the central node of the loading plate (LP) with the surrounding nodes (LL), which ensures equal displacement over the loading area and improved load-deflection prediction, see Figure 7.

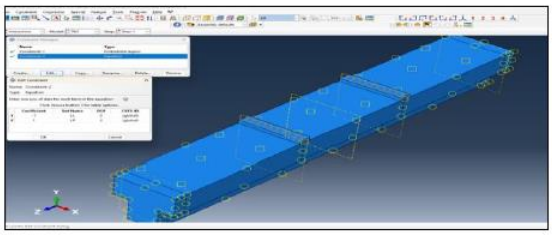

Figure 6. Constraint (Equation)

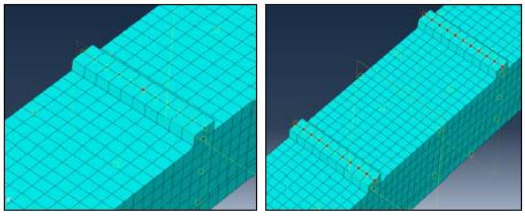

(a) LP **(b) LL**

Figure 7. Sets of Loading Parts

Tie constraints were also implemented to ensure kinematic compatibility between the selected interfaces by connecting the beam surface at the support regions to the corresponding support faces. Steel bearing plates were added at the loading points to reduce local stress concentrations and enhance numerical stability during analysis.

6.8 Boundary Conditions and Loading Scheme

To predict the response of the reinforced concrete T-beam under static loading, corresponding boundary conditions and a loading scheme were assigned to simulate nonlinear structural behavior.

A displacement-controlled loading method was adopted to ensure stable nonlinear analysis, particularly to capture beam deflection, crack initiation, and post-cracking behavior.

For the support conditions, the left end of the beam was modeled as a pinned support. This boundary condition was defined in the initial step and retained throughout the loading step. The horizontal and vertical displacements were restrained (U1 = 0 and U2 = 0), while the remaining degrees of freedom were left unconstrained to represent the behavior of a pinned support.

The right end of the beam was assigned a roller support condition to complete the supported configuration. This boundary condition was also applied in the initial step and maintained throughout the analysis. Only the vertical displacement was constrained (U2 = 0), while the remaining translational degrees of freedom were left unconstrained.

The load was applied at the designated loading point using displacement control, with a downward vertical displacement of -30 mm in the U2 direction. This approach was selected over direct force application to improve numerical convergence and maintain solution stability during nonlinear analysis, particularly after crack formation and stiffness degradation. The loading process was carried out using a static, general analysis step with gradually increasing displacement increments until the target displacement was reached. The displacement-controlled loading technique is particularly suitable for nonlinear analysis of reinforced concrete members, as it allows continuous monitoring of structural response beyond peak load and facilitates accurate evaluation of load–deflection behavior, crack propagation, and failure mechanisms.

6.9 Mesh Generation and Convergence Assessment

The finite element model was discretized into smaller elements to obtain an accurate numerical representation of the structural response under loading. This discretization allows evaluation of response variables at each element's integration points, providing a reliable representation of deformation behavior and load transfer within the structure.

Mid-span deflections were used as the control response parameter to assess the mesh convergence study. Results were in good agreement at coarse mesh densities, and responses began to level off when there were more than 7000 elements. The difference in deflection between the refined meshes was minor, which indicates mesh-independent behavior. Thus, a 25 mm mesh was used for all numerical models, see Figure 8.

A consistent meshing approach was adopted for all specimens to ensure uniformity in the numerical procedure. Mesh density significantly affects solution accuracy and computational efficiency. Therefore, a mesh convergence study was carried out using a reinforced concrete beam model with the same geometry and material properties as the tested specimen. Mid-span deflection was used as the controlling parameter to evaluate mesh sensitivity.

The results showed that the structural response became practically independent of further mesh refinement once the number of elements exceeded approximately 7000, as illustrated in Figure 8. Accordingly, a mesh size of 25 mm was selected as it satisfied mesh-independent results.

In addition, local refinement was applied in high-stress regions, such as supports and loading zones, to improve numerical stability and ensure an accurate representation of stress concentrations and deformation behavior.

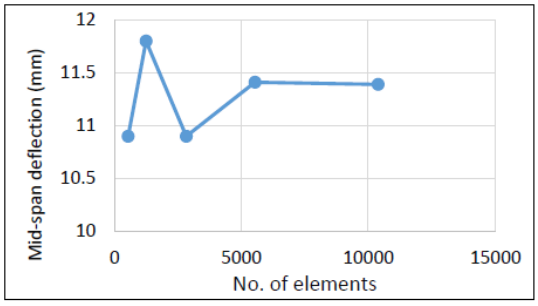

Figure 8. Convergence Study

7. Job and Visualization Module

The finite element analysis was carried out in ABAQUS® 2023 using the Job module, in which the model was submitted for analysis and completed without errors or convergence issues. The computational time depends mainly on mesh density and nonlinear effects, and increases as the model becomes more refined.

After completing the analysis, the results were examined using the Visualization module. This stage facilitated post-processing and interpretation of the numerical outputs, including displacement response, load-deflection behavior, crack development, and failure modes.

The results provide quantitative insight into structural response and enable comparison with experimental data, thereby validating the numerical model.

8. Finite Element Model Validation

The validation of the finite element model was performed by comparing numerical predictions with experimental results for all tested T-beams, with a focus on load-deflection behavior. The results are summarized in Table (5). The comparison was made in terms of ultimate load capacity and deflection response, along with correction factors to quantify the level of agreement between both datasets. In general, the numerical model predicted the load capacity with good agreement. However, it showed larger discrepancies in the deflection response due to the complexity of nonlinear cracking behavior and the assumptions in the material modeling.

Table 5. Numerical and Experimental Results

Beam Designation	Experimental Results		Numerical Results		Load Correction Factor (L*f*)	Deflection Correction Factor (D*f*)
	P_u (kN)	Δ_uE (mm)	P_u (kN)	Δ_uN (mm)	P_uN/ P_uE	Δ_uN/ Δ_uE
B-1	129	12.8	133.93	11.41	1.04	0.89
B-2	113	18	113.94	17.66	1.01	0.98
B-3	174.08	13.2	179.28	13.26	1.03	1.00
B-4	130.5	10	140.43	7.49	1.08	0.75
B-5	143	8.8	142.69	7.35	0.99	0.84
B-6	118	13.8	125.67	10.28	1.07	0.74
Average					1.036	0.86
					(3.6 %)	(13.3%)

9. Ultimate Load Validation

To validate the proposed finite element model, a comparison was made between experimental data and numerical predictions of ultimate load capacity and mid-span deflection. The comparison results showed a close correlation between the two sets of data, indicating good fidelity of the developed ABAQUS model in predicting the overall structural response of foamed concrete T-beams.

The numerical-to-experimental total load ratio (load factor, Lf) ranged from 0.99 to 1.08, with a mean of 1.032, corresponding to an average percentage deviation of about 3.2%. This small variation indicates that the numerical model well predicts the load-carrying capacity of beams globally.

On the other hand, a higher variability was found in mid-span deflection results with the correction factor (Df) ranging from 0.74 to 1.00; an average value of Df is reported by 0.892, counter to an average deviation of around 10.8%. The greater difference between deflection and load capacity may be caused by the complexity of nonlinear cracking behavior in foamed concrete, a perfect bond at the interface between concrete and steel, and the CDP model's sensitivity to stiffness degradation.

Although a deviation between experimental data and predicted results was observed, the overall trend of the experimental and numerical results still indicated a similar pattern, suggesting that the finite element model could be used to predict strength and deformation behavior effectively. Hence, the model is valid enough for further parametric studies.

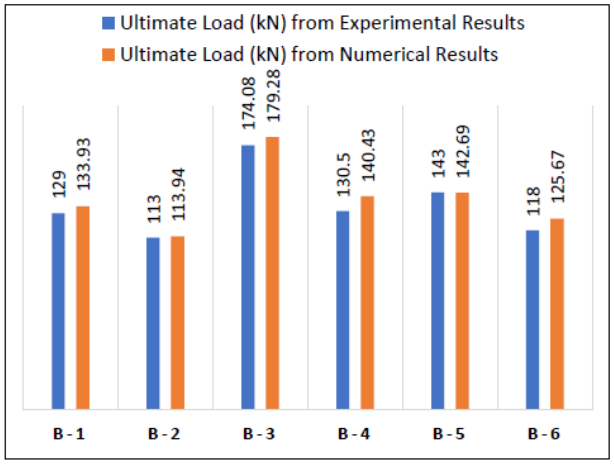

Figure 9. Experimental VS. Numerical Ultimate Load Comparison

10. Load-Deflection Comparison

In this section, a comparison between the numerical and experimental mid-span deflection responses of the specimens was presented. The aim was to evaluate the numerical model's ability to reproduce the actual structural performance of this type of beam. Good agreement was observed between the experimental and numerical results, with both responses exhibiting similar stiffness characteristics, deflection development, and failure behavior. The load-deflection curve comparison further indicated that the proposed numerical method captured the structural behavior of foam concrete T-beams throughout the entire loading process up to failure.

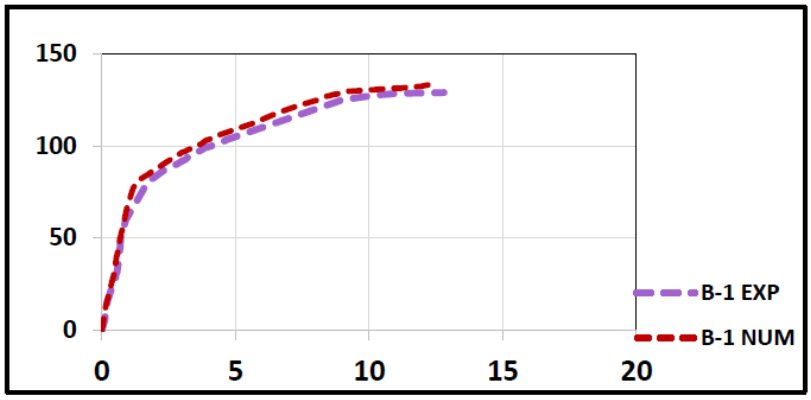

Figure 10. Load-deflection Curve of B-1

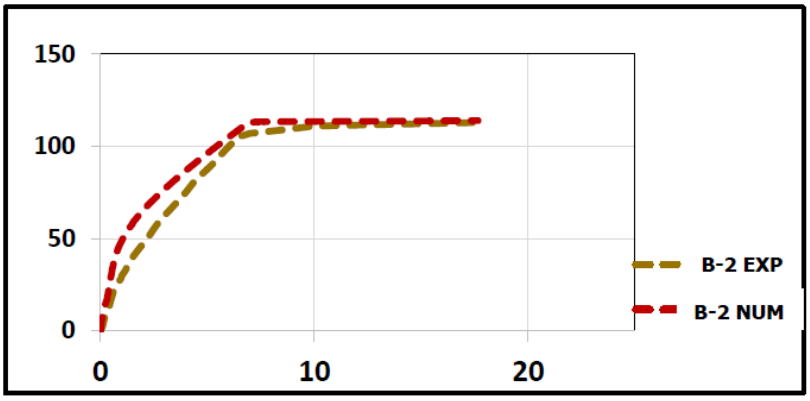

Figure 11. Load-deflection Curve of B-2

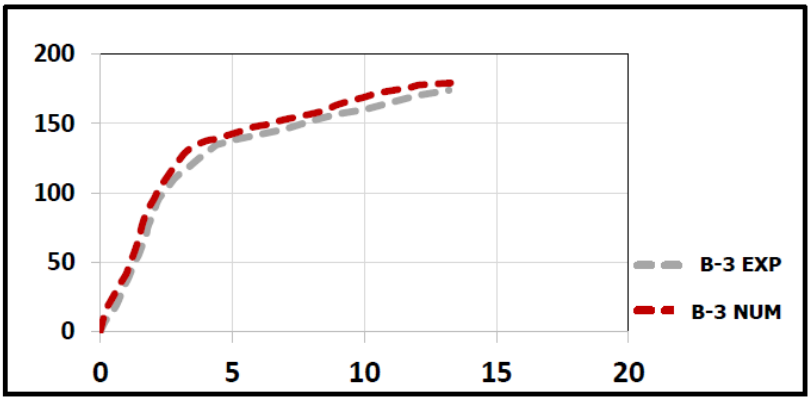

Figure 12. Load-deflection Curve of B-3

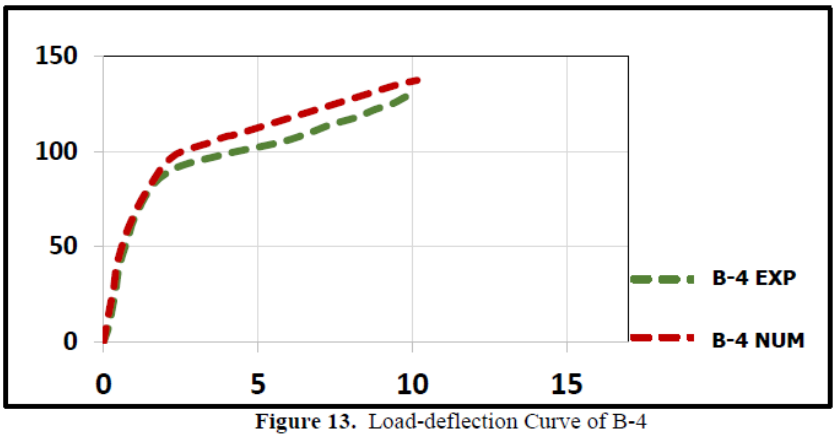

Figure 13. Load-deflection Curve of B-4

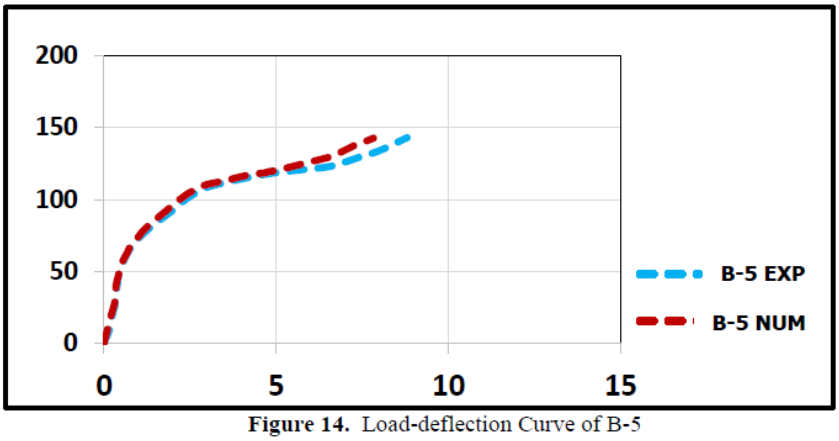

Figure 14. Load-deflection Curve of B-5

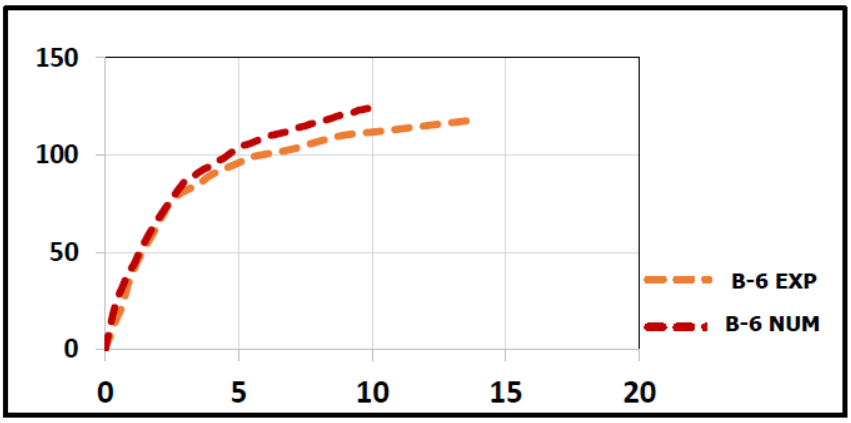

Figure 15. Load-deflection Curve of B-6

11. Crack Pattern

The crack patterns of the foam concrete T-beam specimens were obtained from both the finite element analysis and experimental testing, as shown in Figures (16 to 21). The comparison revealed good agreement in crack initiation, propagation, and distribution for all tested T-beams. This agreement indicated that the finite element model exhibited good accuracy and effectively simulated the cracking process and damage accumulation in foam concrete T-beams subjected to structural loading.

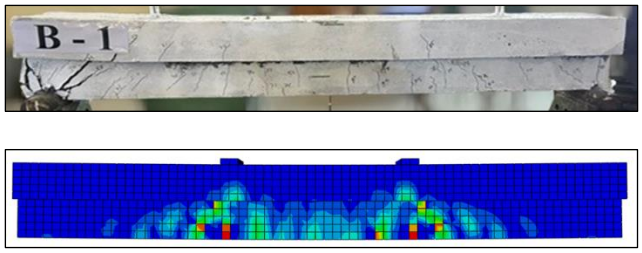

Figure 16. Experimental and Numerical Crack Pattern of B-1

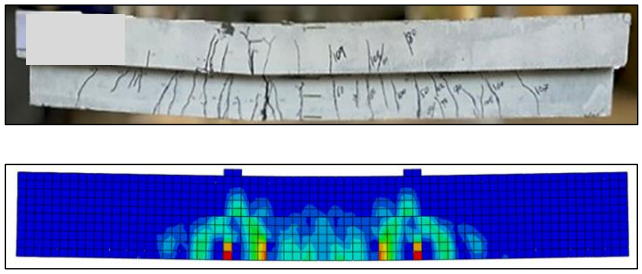

Figure 17. Experimental and Numerical Crack Pattern of B-2

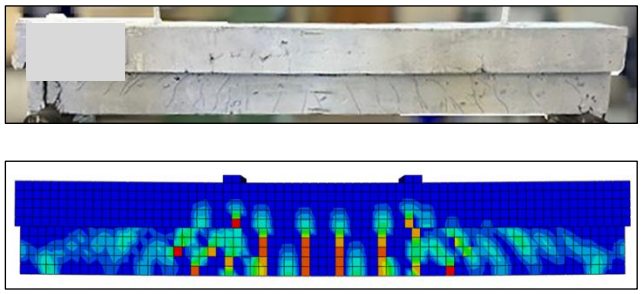

Figure 18. Experimental and Numerical Crack Pattern of B-3

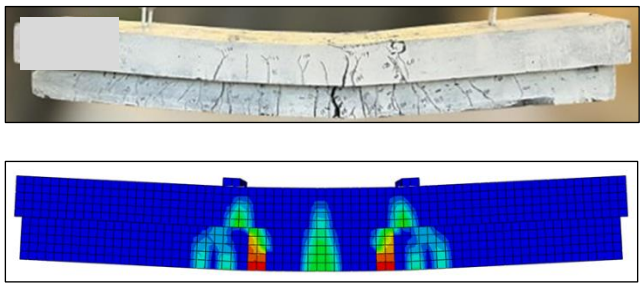

Figure 19. Experimental and Numerical Crack Pattern of B-4

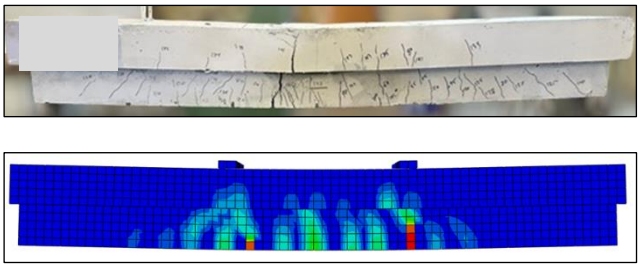

Figure 20 Experimental and Numerical Crack Pattern of B-5

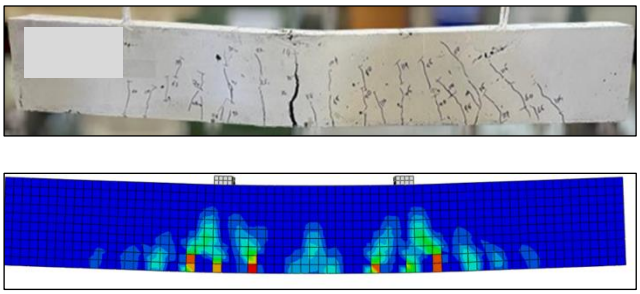

Figure 21. Experimental and Numerical Crack Pattern of B-6

12. Parametric Study

A parametric study was performed to examine the structural behavior of fibered foam-reinforced concrete T-beams under a uniformly distributed load. Whereas the experimental program tested the T-beams under two-point loading, the numerical investigation examined a uniformly distributed loading condition over the beam span, which is of practical application.

These detailed analyses were performed using a parametric study including two groups of specimens. The longitudinal reinforcement ratio was varied in the first group to investigate its effect on T-beam behavior. In contrast, the flange width ratio was varied in the second group. The systematic investigation enabled the assessment of the impact of longitudinal reinforcement and flange width on load-carrying capacity, stiffness, cracking behavior, and overall structural response of FC T-beams under uniformly distributed loading.

13. Results of Parametric Study

The results of the parametric study revealed that changing the loading configuration from two-point to uniformly distributed loading significantly improved the structural performance of all tested T-beams. The increased load capacity at the ultimate state and reduced deflection collectively indicated stiffer behavior and improved energy transfer under distributed loading for most specimens. The ultimate load for the B-1 specimen was increased from 133.93 kN to 151.54 kN (13.1%), accompanied by a reduction of the deflection equal to 41.7%, and severe improvement in load capacity (30.5%) at B-2 accompanied by a reduction of the deflection equal to 51.2%. These same trends were likewise seen for B-4 and B-5.

In contrast, for specimen B-3, the ultimate load decreased by 10.7%, while deflection was reduced strongly (68.1%). This means it can be stiffer in bending but damaging earlier under compression. In theory, this could result from increased reinforcement contribution and redistribution under distributed loading, which may decrease bending concentration but could also hasten compressive failure in the flange zone, thereby reducing the ultimate strength. Specimen B-6 experienced the largest increase in ultimate load (3.1%) and 42% lower deflection compared to Specimen A-6. The findings demonstrated that distributed loading had the potential to improve both efficiency and serviceability of foamed concrete T-beams by reducing deflection and enhancing load-transfer behaviour.

Table 6 Parametric Study Results

Reference Specimen (Numerical)	Two-Points Load		Parametric Specimen (Numerical)	Distributed Load	
	P_u (kN)	Δ_u N (mm)		P_u (kN)	Δ_u N (mm)
B-1	133.93	11.41	B-1-PS	151.54	6.65
B-2	113.94	17.66	B-2-PS	148.72	8.62
B-3	179.28	13.26	B-3-PS	160.01	4.23
B-4	140.43	7.49	B-4-PS	159.27	5.3
B-5	142.69	7.35	B-5-PS	171.65	6.34
B-6	125.67	10.28	B-6-PS	129.6	5.96

14. Conclusion

The findings of this study confirmed that the proposed finite element model has promising predictive capability under the investigated conditions for the structural response of reinforced foamed-concrete T-beams. The numerical results showed very good agreement with respect to the ultimate force capacity: the average experimental and numerical loads were 129.08 kN and 131.78 kN, respectively. This minor difference indicated that the chosen modeling approach accurately captured the behavior of the foamed concrete T-beams. The model produced satisfactory agreement with both the principal load–deflection behavior and crack development. The differences in observed deflection are primarily due to the complex cracking behavior of foamed concrete, material idealization, and assumptions made in the numerical treatment of the element. However, the agreement in crack pattern and failure behavior gives confidence in the validity of the finite element simulation. The parametric study also revealed that a shift from two-point loading to uniformly distributed loading was beneficial for overall structural performance, with higher load capacity and lower deflection generally observed.

References

[1] S. M. Abed, R. A. Hadi, and H. J. Khaliefa, "Improving the mechanical properties of lightweight foamed concrete using various types of fibres," IOP Conference Series: Materials Science and Engineering, vol. 1067, no. 1, Art. no. 012029, 2021, doi: 10.1088/1757-899X/1067/1/012029.

[2] A. J. Njyman and A. A. Hilal, "Mechanical Properties of Hybrid Carbon Fibers Reinforced Modified Foamed Concrete," Iraqi Journal of Civil Engineering (IJCE), vol. 19, no. 1, pp. 60–67, 2025, doi: 10.37650/ijce. 2025.190104.

[3] A. Compaore, J.-Y. N. K. Toure, D. E. P. Klenam, A. S. Merenga, T. K. Asumadu, J. D. Obayemi, N. Rahbar, C. Migwi, and W. O. Soboyejo, "Foam concrete with mineral additives: From microstructure to mechanical/physical properties, workability and durability," Open Ceramics, vol. 23, Art. no. 100812, 2025, doi: 10.1016/j.oceram.2025.100812.

[4] J. F. Castillo-Lara, E. A. Flores-Johnson, A. Valadez-Gonzalez, P. J. Herrera-Franco, J. G. Carrillo, P. I. Gonzalez-Chi, and Q. M. Li, "Mechanical Properties of Natural Fiber Reinforced Foamed Concrete," Materials, vol. 13, no. 14, Art. no. 3060, 2020, doi: 10.3390/ma13143060.

[5] T. Rossetto, D. A. Pohoryles, J. Melo, and H. Varum, "The effect of slab and transverse beams on the behaviour of full-scale pre-1970's RC beam-column joints," in Proc. 16th World Conference on Earthquake Engineering (16WCEE), Santiago, Chile, Jan. 9–13, 2017, Paper No. 3826.

[6] A. M. Issa, M. M. Salem, M. T. Mostafa, H. M. Hadhoud, and H. H. Ghith, "Performance of shear reinforcement against punching shear loads," International Journal of Engineering and Advanced Technology, vol. 9, no. 2, pp. 841–850, 2019, doi: 10.35940/ijeat.b3975.129219.

[7] M. Khalaf, A. El-Shihy, E.-S. El-Kasaby, and A. Youssef, "Numerical estimation and analysis of effective width of composite beams with ribbed slab," International Journal of Application or Innovation in Engineering and Management, vol. 3, no. 8, pp. 1–15, 2014. doi: 10.2648/IJAIEM.120.237.

[8] N. Beningfield, R. Gaimster, and P. Griffin, "Investigation into the air void characteristics of foamed concrete," in Use of Foamed Concrete in Construction, Thomas Telford Ltd., 2005, pp. 51–60, doi: 10.1680/uofcic.34068.0007.

[9] M. Kozlowski, M. Kadela, and M. Gwozdz-Lason, "Numerical fracture analysis of foamed concrete beam using XFEM method," Applied Mechanics and Materials, vol. 837, pp. 183–186, 2016, doi: 10.4028/www.scientific.net/AMM.837.183

[10] O. A. Harry and N. E. Udoh, "Effect of flange width on flexural behavior of reinforced concrete T-beam," Civil and Environmental Research, vol. 8, no. 8, 2016.

[11] P. D. and S. Krishnan, "Equation for the stress-strain curve of concrete," ACI Journal Proceedings, vol. 61, no. 3, doi: 10.14359/7785.

[12] T. T. C. Hsu and Y. L. Mo, Unified Theory of Concrete Structures. 2010. doi: 10.1002/9780470688892.